ACS APPLIED MATERIALS & INTERFACES

Research Article

Cite This: ACS Appl. Mater. Interfaces 2019, 11, 19819−19829

www.acsami.org

Modulation of Cellular Colonization of Porous Polyurethane Scaffolds via the Control of Pore Interconnection Size and Nanoscale Surface Modifications

G. Lutzweiler,[*,†,‡,§] J. Barthes,[∥] G. Koenig,[†,‡] H. Kerdjoudj,[#,¶] J. Mayingi,[⊥] F. Boulmedais,[§] P. Schaaf,[*,†,‡] W. Drenckhan,[§] and N. E. Vrana[*,∥]

[†]Institut National de la Santé et de la Recherche Medicale, UMR_S 1121, 11 rue Humann, 67085 Strasbourg Cedex, France

[‡]Faculté de Chirurgie Dentaire, Université de Strasbourg, 8 rue Sainte Elisabeth, 67000 Strasbourg, France

[§]Université de Strasbourg, CNRS, Institut Charles Sadron, 23 rue de Loess, 67034 Strasbourg, France

[∥]Protip Medical SAS, 8 Place de l'Hôpital, 67000 Strasbourg, France

[⊥]Cetim Grand Est, 24a Rue d'Alsace, 67400 Illkirch-Graffenstaden, France

[#]EA 4691, Biomatériaux et Inflammation en Site Osseux (BIOS), SFR-CAP Santé (FED4231), Université de Reims Champagne Ardenne, 51100 Reims, France

[¶]UFR d'Odontologie, Université de Reims Champagne Ardenne, 51100 Reims, France

Supporting Information

ABSTRACT: Full-scale cell penetration within porous scaffolds is required to obtain functional connective tissue components in tissue engineering applications. For this aim, we produced porous polyurethane structures with well-controlled pore and interconnection sizes. Although the influence of the pore size on cellular behavior is widely studied, we focused on the impact of the size of the interconnections on the colonization by NIH 3T3 fibroblasts and Wharton's jelly-derived mesenchymal stem cells (WJMSCs). To render the material hydrophilic and allow good material wettability, we treated the material either by plasma or by polydopamine (PDA) coating. We show that cells weakly adhere on these surfaces. Keeping the average pore diameter constant at 133 μm, we compare two structures, one with LARGE (52 μm) and one with SMALL (27 μm) interconnection diameters. DNA quantification and extracellular matrix (ECM) production reveal that larger interconnections is more suitable for cells to move across the scaffold and form a three-dimensional cellular network. We argue that LARGE interconnections favor cell communication between different pores, which then favors the production of the ECM. Moreover, PDA treatment shows a truly beneficial effect on fibroblast viability and on matrix production, whereas plasma treatment shows the same effect for WJMSCs. We, therefore, claim that both pore interconnection size and surface treatment play a significant role to improve the quality of integration of tissue engineering scaffolds.

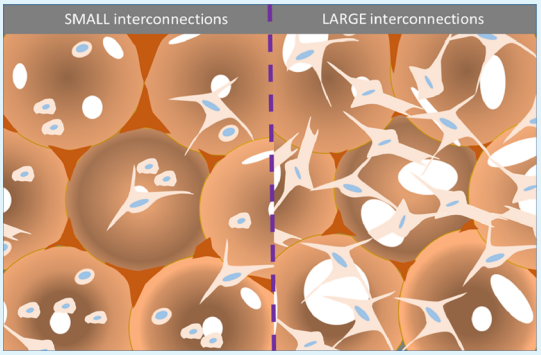

KEYWORDS: *polyurethane scaffold, Wharton jelly mesenchymal stem cells, interconnected pores, surface modification, dopamine*

1. INTRODUCTION

As they are used for withstanding the mechanical constraints of a tissue or an organ to be replaced, a tissue engineering scaffold should allow cell migration and proliferation into its empty volumes, favor intercellular exchanges, and production of extracellular matrix (ECM).[1] 3D porous scaffolds, which fulfill these requirements,[2,3] are manufactured using different types of material, such as metals, ceramics, and natural or synthetic polymers.[4,5] They need to be well interconnected to allow cell migration through the whole structure and to guarantee good oxygen and nutrient supply as well as removal of metabolic wastes.[6,7] Many techniques were employed to generate such structures, for example, particle leaching,[8] gas foaming,[9] freeze drying,[10] or 3D printing.[11] The influence of the pore size on cell behavior in porous structures has been widely studied.[12−15] However, the great diversity of manufacturing techniques, the cell type, material, and culture conditions differ from one study to another rendering difficult to draw conclusions on what can be the optimal scaffold. Pamula et al.[16] generated poly(lactic-*co*-glycolic acid) (PLGA) scaffolds, having three different pore sizes 40, 200, and 600 μm. They demonstrated that osteoblast-*like* MG63 migration was improved in scaffolds with pore size

Received: March 14, 2019
Accepted: May 10, 2019
Published: May 10, 2019

DOI: 10.1021/acsami.9b04625
ACS Appl. Mater. Interfaces 2019, 11, 19819−19829

of 600 μm compared to 40 and 200 μm. Stenhamre et al.[17] showed that for human chondrocytes seeded on polyurethane (PU) scaffolds, chondrogenesis markers (i.e., glycoaminoglycans, GAGs, and type II collagen) were upregulated in scaffolds having the smallest pore size (i.e. <150 μm) compared to larger ones (300−500 μm). Conversely, rat mesenchymal stem cells seeded on collagen-hyaluronic scaffolds secreted more sulfated GAGs, type II collagen, and showed a higher SOX9 expression in structures with pore diameter of 300 μm compared to 94 or 130 μm.[18] Although information on the optimization of the pore size for a given cell type is available, the influence of interconnection size between two adjacent pores in porous structures on cell behavior has been more rarely investigated, which is the focus of the current study.

For example, supercritical foamed scaffolds were generated using different molecular weight PLGA, giving structures with different distributions of pore and interconnection diameters.[19] However, the change in pore size was accompanied by a systematic change in the interconnection size, making it impossible to draw solid conclusions about the specific influence of either of the parameters. In another study, bone marrow stromal cells (MSCs) were seeded on two hydroxyapatite scaffolds, with interconnection sizes of more than 200 μm for a first group and below 100 μm for a second group, and subsequently implanted subcutaneously in mice.[20] The authors reported that interconnection size has a significant effect on the diameter of blood vessels formed within the scaffold. Yet, the fabrication processes of the different scaffolds used were not the same, and the resulting structures were different. Results may, thus, have been influenced by other factors than the interconnections only.

Separation and fine control of both interconnection and pore sizes cannot be achieved in all fabrication processes. "Sphere templating" gives an explicit control over the size of the pore interconnections while keeping the chemical nature of the material constant. The principle of this method is based on a sacrificial porogen agent packed in a container on which an initial liquid material is poured in order to fill the space between the porogen particles. Once the liquid phase is solidified, the porogen is dissolved and removed, leaving a porous structure whose architecture can be precisely controlled via the geometrical properties of the porogen (Figure 1A). Spherical particles of poly(methylmethacrylate)[21] or paraffin[22] are commonly used as porogens.

PU is known for its biocompatibility and is widely used for tissue engineering applications.[23,24] However, many authors reported the use of coatings or modifications in the formulation during the PU synthesis in order to increase the affinity of cells for the surface. e.g., Li et al.[25] seeded MSCs onto a fibrin−PU hybrid scaffold to improve cell retention after seeding and to obtain a homogenous distribution throughout the scaffold.

Li and Huang[26] grafted type I collagen onto PU surfaces to increase the hydrophilicity of the substrate as well as cell attachment. In another study, Lin et al.[27] grafted RGD peptide sequences onto a PU backbone in order to improve endothelial cell adhesion.

Another promising coating is dopamine, a chemical close to the adhesive molecules found in mussels.[28] It can self-polymerize to form thin polydopamine (PDA) films, which adhere on almost any type of surface. PDA films are easy to process because the coating is done by simply dipping the sample in a solution. PDA coating was already employed to improve cell adhesion and proliferation.[29,30]

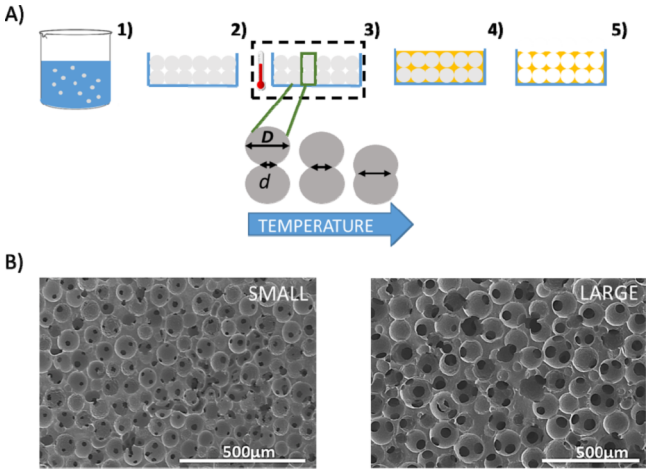

Figure 1. (A) (1) Paraffin sphere generation by an emulsion dispersion method, (2) paraffin sphere packing in a Petri dish followed by (3) sintering in a mold at various temperatures, (4) polymer solution is poured on the top to infiltrate between beads and (5) paraffin dissolution in solvent. (B) SEM images of the resulting scaffold with SMALL and LARGE interconnections.

In this paper, we study the influence of interconnection size of a porous PU material supplemented with different surface functionalizations on cell colonization. For this purpose, we first produced by sphere templating two types of structures with identical pore size but with different interconnection diameters. Bare PU scaffolds appeared extremely hydrophobic, preventing the penetration of aqueous solutions and then cell suspension. Hence, PU scaffolds were functionalized to render them more hydrophilic by both PDA and plasma treatments. The functionalized structures were seeded with two cell types: NIH 3T3 fibroblasts to study cell migration and distribution and Wharton's jelly-derived mesenchymal stem cells (WJMSCs) as a potential cell source for chondrogenesis for cartilage tissue engineering. Therefore, we investigated the combination of surface chemistry with the architecture of the scaffold on cell colonization. Although surface chemistry could promote or prevent cell survival and colonization with regard to the cell type, the diameter of the interconnections appeared to be a key feature for supporting the organization of cells in a three-dimensional way and to improve their viability.

2. MATERIALS AND METHODS

2.1. Generation of PU Scaffolds of Well-Controlled Structures. We generated porous PU scaffolds by a sphere templating method whose basis was already described elsewhere[22,31] and which we fine-tuned in order to obtain the desired structural features in a highly reproducible manner. As sketched in Figure 1A, 10 g of pure paraffin wax (Fisher Scientific, mp 58−62 °C) is put in a solution of 40 mL of water and 3 g of polyvinyl alcohol (PVA, Sigma) at 70 °C. Being liquid at this temperature, the paraffin is emulsified into small droplets under stirring with a magnetic stirrer at 950 rpm. After 10 min of stirring, 400 mL of ice-cold water is poured in the mixture to quench the paraffin drops in order to obtain spherical particles. The paraffin beads are then rinsed with distilled water and sieved to select the desired size range (125−200 μm) from the polydisperse sphere distribution. The paraffin beads are then left to dry under a fume hood for 24 h. The dried paraffin beads are packed in a Petri dish (35 mm diameter, VWR) with holes that are initially covered with parafilm to prevent the loss of particles. The ensemble is

DOI: 10.1021/acsami.9b04625
ACS Appl. Mater. Interfaces 2019, 11, 19819−19829

then placed in an oven (Memmert) at 43 °C in order to sinter the beads. They are left in the oven for 20 min in the case of the structure with SMALL interconnections, and for 1 h for LARGE interconnections. The size of the interconnections is related to the heating time as shown in Figure 2. Therefore, by keeping the paraffin beads longer in the oven, one can obtain larger interconnections for a given bead diameter.

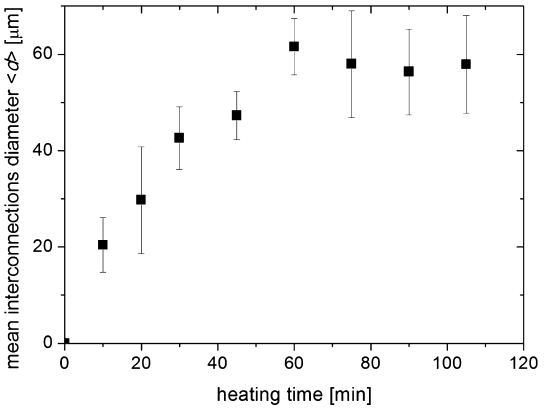

Figure 2. Evolution of the interconnection diameter against heating time for paraffin beads having an average diameter of 133 ± 28 μm heated up to 43 °C.

Once sintering is finished, the molds are taken out of the oven and left to cool at room temperature. The PU premix is made by mixing a polyol (polyether triol Voranol 6150, Dow) with an isocyanate [poly methylene diphenyl diisocyanate (MDI), Voranate M220, Dow] at a weight ratio of 3.57−1. Both are mixed with an ULTRA-TURRAX (IKA T25) at 15 000 rpm to obtain a homogenous mixture. This mixture is then cast on top of the mold containing the sintered paraffin beads so that it fills progressively the space between the beads. For this purpose, the parafilm that plugged the holes in the Petri dish is removed to make sure that the air entrapped in the structure can escape. The polymer matrix is then left to solidify for 48 h. The paraffin beads are then dissolved using Soxhlet extraction with n-hexane as the solvent for 4 h at 80 °C. Finally, the porous structure is let in an oven for 12 h at 40 °C to let the remaining solvent to evaporate.

2.2. Porosity Measurement. Porosity was assessed as described elsewhere[32] using the following formula

$$P\ (\%) = \left[1 - \frac{\rho_p}{\rho_b}\right] \times 100 \tag{1}$$

where ρ_p and ρ_b are the density of the porous and the bulk polymer, respectively. The densities were obtained by preparing pure polymer solid and the scaffolds of the same volume and weighting them in order to obtain the density ratio.

2.3. Hydraulic Permeability Measurement. The hydraulic permeability of the samples to water was measured using a gravimetric method described elsewhere.[33] In brief, the porous sample cut into a disc shape of thickness H was placed to fill the entire passage of a U-shaped apparatus (Scheme 1). A valve allows to generate a water height difference Δh (i.e., a pressure gradient $\Delta P = \rho g \Delta h$, where ρ is the density of water and g the gravitational acceleration), which, when opened, gives the driving force for the water to flow across the sample. Because the PU was hydrophobic, we added 1% wt of silicone surfactant (TEGOSTAB 8002, Evonik) to the water to ensure that the scaffold is completely wet. The surfactant does not influence the flow properties. We measured the velocity, V_D ("Darcy velocity"), at which the water passes through the sample over a range of ΔP. Both are related by Darcy's law[34]

Scheme 1. Principle of the U-Shaped Apparatus Used for Water Hydraulic Permeability Measurement

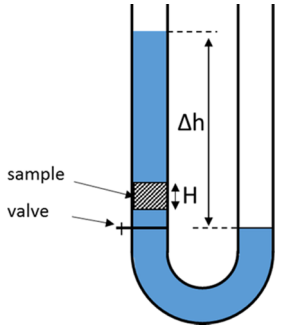

$$V_D = -k\frac{\rho g}{\eta}\frac{\Delta h}{H} \tag{2}$$

where η is the dynamic viscosity of water (taken as 10^{-3} Pa·s) and k is the hydraulic permeability (in cm^2). We, thus, obtain k by taking the slope of the V_D (Δh) curve and multiplying it by the $\eta H/\rho g$.

2.4. Mechanical Characterization. Typical stress−strain curves were obtained with a standard rheometer (Kinexus Ultra+, Malvern). Samples were cut into discs (26 mm in diameter, 5 mm height) and preloaded with 0.5 N, which was considered as the force when the plate was in contact with the surface of samples. The samples were compressed until 20% strain. Young's modulus was calculated from the slope of the obtained stress−strain curves.

2.5. Functionalization of the PU Surface. PDA coating was performed by dipping the porous sample into a solution of 2 mg/mL of dopamine hydroxychloride (Sigma) dissolved in 10 mM Trizma base hydroxychloride at pH 8.5 under gentle stirring for 24 h. Samples were then rinsed several times with distilled water and left to dry for 12 h at room temperature under a fume hood. Plasma treatments of PU samples were carried out by placing the sample in the chamber of a plasma cleaner using ambient air (Harrick Plasma PD-32G-2) at 200 mTorr for 3 min for each face. Samples were then directly seeded with the cell suspension in order to prevent hydrophobic recovery.

2.6. Quantification of Secreted ECM. Collagen and non-collagenous proteins secreted by cells were quantified using the Sirius Red/Fast Green Collagen Staining Kit (Chondrex, Inc.). Scaffolds seeded with cells were first rinsed in phosphate-buffered saline (PBS) two times, then the samples were immersed in dye solution for 30 min. Afterwards, the samples were rinsed with distilled water several times until the water became clear. Porous scaffolds were then immersed in 1 mL of dye extraction buffer for 15 min. The solution (100 μL) was collected in a 96-well plate, and absorbance values at 540 and 605 nm were recorded with a spectrophotometer. The collagenous and noncollagenous parts were calculated with the equation given in the kit protocol

$$\text{Collagenous part } (\mu\text{g of protein/mg of material}) = \frac{(\text{OD}_{540\text{nm}} - (\text{OD}_{605\text{nm}} \times 0.291)}{0.0378 \times \text{scaffold weight}} \tag{3}$$

$$\text{Non-collagenous part } (\mu\text{g of protein/mg of material}) = \frac{\text{OD}_{605\text{nm}}}{0.00204 \times \text{scaffold weight}} \tag{4}$$

$\text{OD}_{540\text{nm}}$ and $\text{OD}_{605\text{nm}}$ are the optical density at 540 and 605 nm, respectively. Scaffolds were weighted before seeding to quantify the amount of proteins relative to the amount of material.

2.7. Cell Culture and Seeding. PU scaffolds were cut into cylinders of 1 mm height and 13 mm diameter. Samples were sterilized in 70% ethanol overnight and placed under UV radiation, 15 min for each face for sterilization. The constructs were then placed in a 24-well plate. For the flat surface experiments, the PU was cast on the bottom of a 6-well plate and left to polymerize. Once solidified,

DOI: 10.1021/acsami.9b04625
ACS Appl. Mater. Interfaces 2019, 11, 19819−19829

PDA-coating was performed as previously described. The PU treated with plasma was taken out of the well plates to be placed under the plasma cleaner for 3 min and put back in the wells. Murine fibroblasts NIH 3T3 (ATCC) were first cultured in T175 flasks in Dulbecco's modified Eagle's media supplemented with 10% (v/v) of decomplemented fetal bovine serum (FBS) and 1% penicillin/streptomycin (v/v) in a humidified incubator (5% CO_2, 37 °C). WJMSCs were harvested from four consenting patients with a procedure described elsewhere[35] [authorization body: Inserm, ITMO Santé Publique Pôle Recherche Clinique (PRC), authorization number: DC-2015-2364] and cultured in T175 flasks, in α-MEM Eagle (Gibco) supplemented with 20% of decomplemented FBS, 1% penicillin/streptomycin/amphotericin, and 1% of L-glutamine. Once cells reach about 70−80% confluence, cells were washed with PBS, and passaged with trypsin−ethylendiaminetetraacetic acid (EDTA) solution. WJMSCs were seeded at passage 4, whereas fibroblasts were seeded at passage 8. Cell seeding was achieved by deposing a 150 μL drop on the top of each scaffold at a density of 1×10^6 cells per scaffold. The media (2 mL) was finally added in each well, and media was changed each 2 days during the experiment. All experiments were conducted in hydrophobic coated well plate.

Hydrophobic 12-well plates were prepared as follows: 350 μL of poly(2-hydroxyethyl methacrylate) (Sigma-Aldrich, P3932) solution at 0.5% (w/v) in ethanol was incubated in each well plate and put in incubator at 39 °C for 24 h until complete evaporation of ethanol. Then, culture plates were sterilized for 15 min under UV before use.

2.8. DNA Quantification. Scaffolds with cells were crushed and immersed in a lysis extraction buffer [10 mM tris-HCl, 1 mM of EDTA (Sigma), and 0.1% v/v of Triton X-100 (Euromedex, France) in sterilized water pH 8]. The solution was placed in a 10 mL falcon tube in a freezer at −80 °C overnight. DNA purification was performed by the phenol/chloroform method. The lysed cells solution (200 μL) was poured in a 2 mL tube, and an equal volume of phenol/chloroform/isoamyl alcohol 25:24:1 (Sigma-Aldrich) solution was added to the solution. The mixture was vortexed for 20 s 10 times, and centrifuged at 13 000 rpm at 4 °C for 5 min. The aqueous phase was extracted by careful pipetting and placed in a new 2 mL tube. Again, an equal volume of phenol/chloroform/isoamyl alcohol 25:24:1 solution was added, and the operation was repeated. After centrifugation, the supernatant was pipetted and poured in a new tube, in which an equal volume of pure chloroform (Sigma) was added, the mixture was vortexed again for 20 s 10 times and centrifuged at 13 000 rpm for 5 min. DNA was precipitated by adding 150 μL of 5.5 M sodium acetate and two times volume of 100% ethanol was added. The tubes were placed at −20 °C overnight. Samples were vortexed for 20 min at 4 °C at 13 000 rpm, and the supernatant was removed, leaving the pellets at the bottom of the tubes. Samples were washed in 80% ethanol, vortexed three times, and centrifuged at 13 000 rpm. Ethanol was removed, and tubes were let under a fume hood for the complete evaporation of ethanol for 20 min. Buffer solution (200 μL, 10 mM tris-HCl and 1 mM of EDTA (Sigma) pH 8) was added to solubilized DNA pellets and DNA concentration (μg/mL) was read on a NanoDrop device. The value was divided by the scaffold weight to get a DNA concentration relative to the material amount to account for the difference from one sample to another.

2.9. Contact Angle Measurement. Surface wetting properties of the raw PU, plasma-treated, and PDA-coated samples were obtained by static contact angle measurements with purified water (Milli-Q) using the sessile drop technique (Attension Theta, Biolin Scientific). The contact angles were obtained by image treatment using the software OneAttension.

2.10. Scanning Electron Microscopy. Samples were observed with scanning electron microscopy (SEM, Hitachi SU8010) under 1 keV voltage acceleration to investigate the structural properties of the samples in general, and the dimensions of the pores and interconnections in particular. Images were treated and analyzed with ImageJ software.[36] The pore dimensions were obtained by measuring at least 100 pores by hand and taking the average. The size of the black interconnections (see Figure 1B) was obtained by employing the "particle analysis" tool after thresholding the image with a selected circularity of 0.5. Because the interconnections are viewed at different angles, the circular holes appear as ellipses. Their true diameter was approximated by the Feret's diameter, which is the longest axis of the ellipse and which corresponds to the diameter of the circle.

2.11. Optical Microscopy. Images of cells on flat surface were taken with an optical inverted microscope (Eclipse, TS100, Nikon) mounted with a digital camera (DS-Fi2-L3, Nikon).

2.12. Confocal Microscopy. Both cell types within scaffolds were observed with a confocal microscope (Zeiss LSM 710). For staining the cells, cells in the scaffolds were fixed in a 4% paraformaldehyde solution in PBS, for 30 min at ambient temperature. Thereafter, the samples were washed with PBS, and the cell membrane was permeabilized with a solution of 0.1% Triton X-100 in PBS for 10 min, followed by two washing steps with PBS, and incubated with a solution of 1% v/v of bovine serum albumin for 20 min. The actin filaments of cells in scaffolds were then stained with a solution of fluorescent molecule-conjugated phalloidin (Alexa Fluor 568) at 1/40 v/v in PBS for 1 h. Afterwards, samples were washed two times with PBS for 5 min, and subsequently incubated in a 4′,6-diamidino-2-phenylindole (DAPI, PromoKine) solution in a concentration of 1/100 in PBS for 5 min. At the end, samples were washed two times in PBS for 5 min and kept in PBS at 4 °C before the microscopic observation.

2.13. Statistical Analysis. For data of the DNA and ECM, quantification are expressed as the average value and the bars indicate the standard deviation (SD). Two ways (ANOVA) was performed followed by the Holm−Sidak method to account for all pairwise multiple comparisons. p values < 0.05 were considered significant.

3. RESULTS AND DISCUSSION

3.1. Morphology and Permeability of PU Scaffolds. Porous PU scaffolds were generated by a sphere templating method using spherical paraffin beads at the desired dimensions. After synthesis and sieving of 133 μm diameter paraffin beads, they were packed in a Petri dish and were sintered at 43 °C for two different times to create a neck of tunable cross-section between adjacent particles (Figure 2). After cooling, a mixture of polyol and isocyanate was casted on the Petri-dish. After 48 h, the paraffin beads were dissolved with hexane.

PU porous scaffolds were produced with an average pore size of 133 ± 28 μm and with two pore interconnection sizes depending on the sintering time of paraffin beads (Figure 1B).

For a sintering time of paraffin beads of 20 min, average interconnection diameter $\langle d \rangle$ of the resulted scaffold was 27 ± 10 μm, named SMALL scaffold (Figure 1B, left). With a sintering time of 1 h, the average diameter $\langle d \rangle$ was 52 ± 12 μm, named LARGE scaffold (Figure 1B, right). The spherical footprint of the paraffin template allows to keep a homogenous geometry across the entirety of both samples. The backbone of the polymer was polyether-based to reduce hydrolysis and, therefore, to maintain the integrity of the scaffold for the whole experiment. PU scaffold porosity increases with the interconnection sizes from 60% for SMALL to 81% for LARGE scaffolds. Young's modulus was shown to be higher for the scaffold having SMALL interconnections; we found E = 284.4 kPa for SMALL interconnections, and E = 239 kPa for LARGE interconnections (Figure S4). However, mechanical tests were performed by compressing the whole scaffold, thus, mechanical response is a macroscopic response of the scaffold; at the cell level, cells may only sense the local modulus of the PU, which was the same for all samples. Because the sintering of the paraffin beads leads to larger neck formation (i.e., larger

DOI: 10.1021/acsami.9b04625
ACS Appl. Mater. Interfaces 2019, 11, 19819−19829

interconnections), there is less space available for PU penetration in the interstitial space and then more void space after paraffin beads dissolution, leading to more porous structures. Aqueous permeability of PU scaffolds was also investigated by measuring the hydraulic permeability (Section 2.3 in Materials and Methods section). The values obtained for LARGE scaffolds are an order of magnitude larger than those for SMALL ones (Table 1). Similar values in term of hydraulic

Table 1. Summary of the Properties of Scaffolds Used for Cellular Studies

structure name	mean pore diameter $\langle D \rangle$ [μm]	mean interconnection diameter $\langle d \rangle$ [μm]	porosity P [%]	permeability k [cm^2]
LARGE	133 ± 28	52 ± 12	81 ± 13	5×10^{-6}
SMALL	133 ± 28	27 ± 10	60 ± 11	4.5×10^{-7}

permeability were found by Chor and Li[37] for PVA scaffolds with nearly the same pore diameter (150 μm) as we found in the case of LARGE interconnections. The dependence of the hydraulic permeability ⟨k⟩ on the interconnection diameters was reported by Marshall and Ratner[33] who provided a model where the hydraulic permeability increases with the square of the interconnection radius. Moreover, Kemppainen and Hollister[38] designed 3D printed poly(ε-caprolactone) (PCL) scaffolds with tailored interconnection diameter with different hydraulic permeability, where they demonstrate that interconnection size is a key parameter for transport properties throughout the scaffold.

3.2. Functionalization of PU Scaffolds. Aqueous solutions deposited on top of a bare PU material present a high contact angle and do not penetrate into the scaffold due to its hydrophobicity. We thus functionalized the material either by exposition to plasma or by bringing it in contact with a dopamine solution in order to create a thin PDA coating on the porous scaffold. The hydrophobic character of flat PU surfaces was confirmed by contact angle measurement (Figure 3A) with a contact angle of 95°. It decreased continuously for 7 min upon exposure to plasma before reaching an equilibrium value around 35°. It is known that plasma treatment induces cleavage of polymer chains, which promotes the formation of free radicals and highly reactive species that mostly react with oxygen or water vapor to form hydroxyl groups.[39,40] These polar groups increase the wettability of the PU as shown by a decrease of the contact angle values. Yet, a rapid hydrophobic recovery of the surface was observed after plasma treatment due to re-arrangement of polymer chains that expose the hydrophobic part toward air.[41] As seen on Figure 3B, after only 5 min, contact angle rises from 35° to 48° and stabilizes around 60° for longer times.

In order to achieve a permanent improvement of the scaffold wettability, PDA coatings were deposited on PU. Dopamine is known for its ability to stick on many types of surfaces and to self-polymerize to give thin film depositions. The surface modification is versatile and easy to process because the sample coverage is obtained by a simple dipping step, as explained in the Materials and Methods section (see Section 2.4). After PDA deposition, aggregates were observed on PU scaffolds, as reported in other studies (Figure 4A).[42] Surface hydrophilicity of PDA-treated PU surfaces greatly increases after 3 h of dipping and continues to increase slightly for longer dipping durations (Figure 4B). A change of color is observed proving PDA deposition on the whole surface (Figure 4B insets). Unlike plasma treatment, PDA coating shows a much better stability with time with regard to the wetting properties remaining stable for 48 h (Figure 4C), instead of only 5 min for plasma treatment (Figure 3B).

3.3. Cell-Growth in Porous Samples. Cells were brought in contact with PU scaffolds functionalized by plasma treatment and with PDA. In the case where we functionalized the PU scaffold by plasma treatment, as the hydrophilicity decreases with time, we seeded the cells immediately after plasma exposure for studying the effect of the interconnection diameter. We quantified the DNA, the collagen, and the noncollagenous contents such as GAG after 14 and 21 days of culture. As matrix production is a slow process, collagenous and noncollagenous secretions were not quantified before day 14; furthermore, it guarantees to be above the detection limit of the quantification kit. DNA content reflects the number of cells present in the scaffold. In order to avoid as much as possible, the presence of dead cells that will contribute to DNA content, we thoroughly rinsed the scaffold before each measurement. Collagen and noncollagen contents reflect the ECM produced by the cells. The results are summarized on Figure 5 for NIH 3T3 cells and in Figure 6 for WJMSCs. One first observes that the two cell types respond differently to the functionalization method.

DNA quantification of fibroblasts, illustrated in Figure 5A, did not show significant variation of measured values over the studied time for PDA-treated scaffold but showed a significant decrease for plasma. Furthermore, collagen and noncollage-

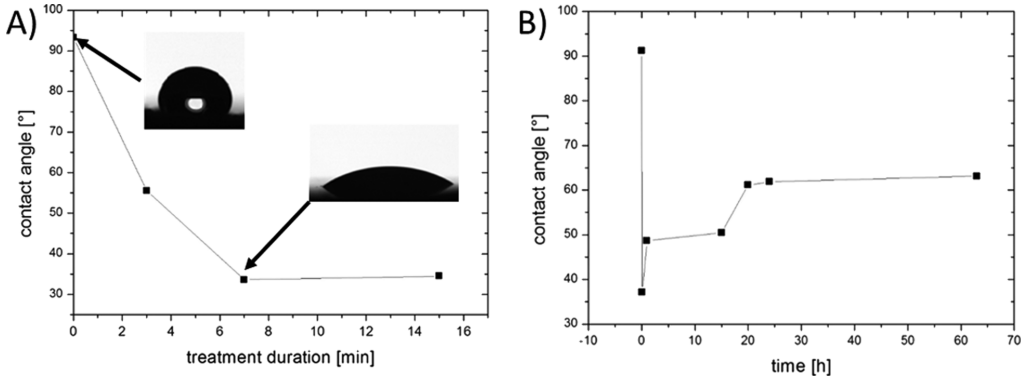

Figure 3. (A) Water contact angle measurement on PU flat surface after various treatment durations. (B) Water contact angle measurement as a function of time after plasma treatment.

DOI: 10.1021/acsami.9b04625
ACS Appl. Mater. Interfaces 2019, 11, 19819−19829

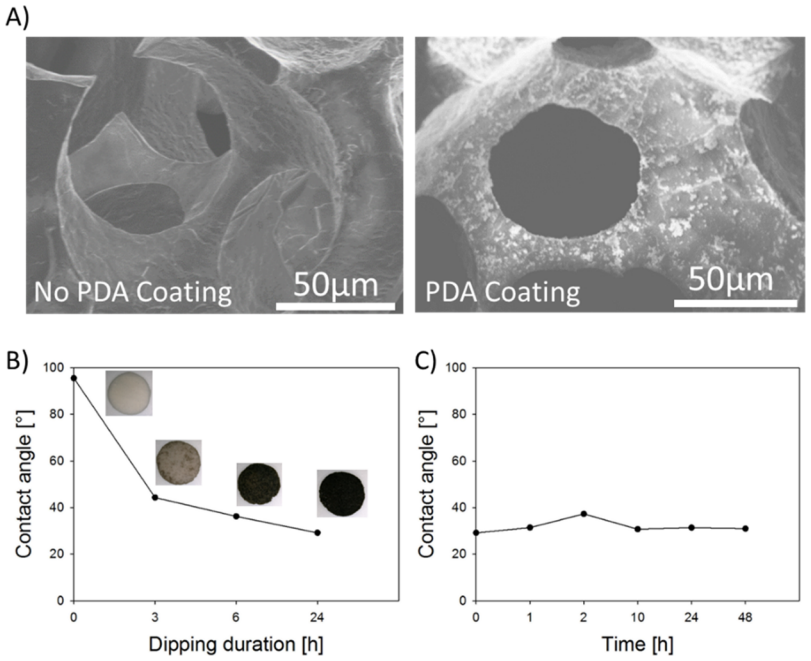

Figure 4. (A) SEM images of PU scaffold with and without PDA coating for 24 h, (B) contact angle measurement of PDA-coated PU flat surfaces with various dipping times, and (C), contact angle evolution with time after PDA treatment on PU dipped in PDA solution for 24 h.

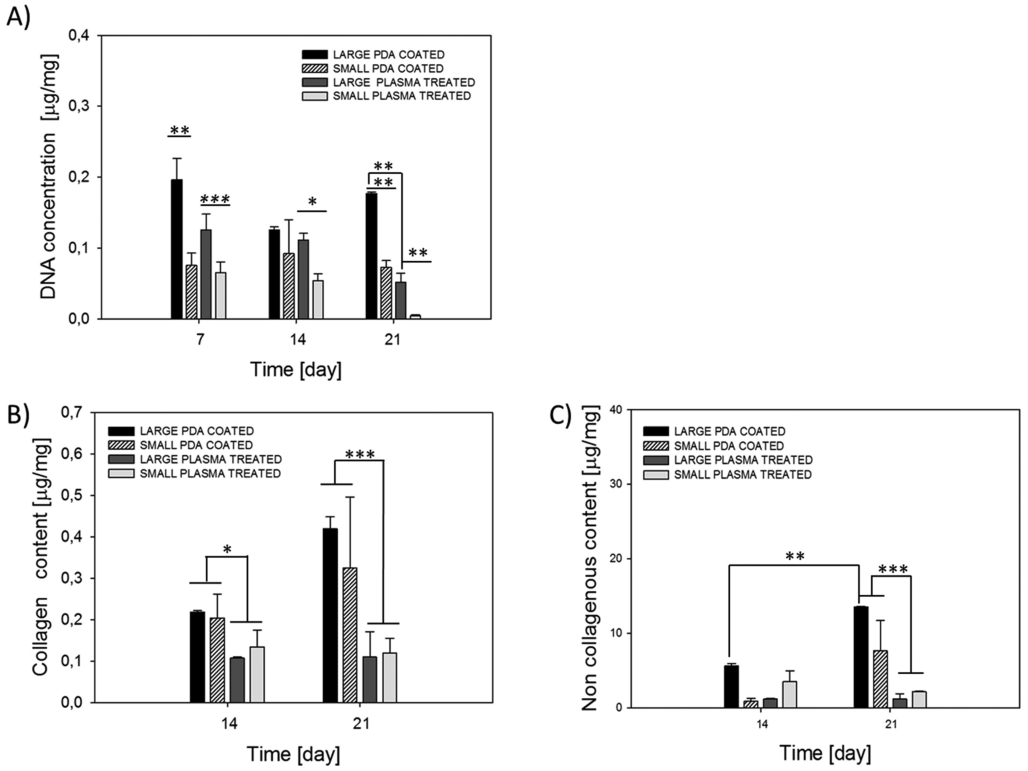

Figure 5. (A) DNA quantification of NIH 3T3 in PU scaffolds, either coated with PDA or just treated with plasma (B) collagen secreted quantification in PU scaffold and (C) noncollagenous content secretion, values expressed as mean ± SD $n = 3$ $^{*}p < 0.05$, $^{**}p < 0.01$.

nous contents are significantly higher on PDA-coated samples after 14 and 21 days of culture, respectively, compared to plasma-treated samples for a given interconnection size Figure 5B,C.

In contrast to fibroblasts, WJMSC behavior is better on plasma-treated PU scaffold compared to PDA. For fibroblasts, the ECM production is favored on PDA-coated samples in comparison to plasma-treated ones. As far as DNA content is concerned, it remains fairly constant overtime for PDA-treated samples (compare D7 to D21) and it decreases for plasma-treated samples. This indicates that on PDA-treated samples, the number of cells remains fairly constant over time. For WJMSCs, DNA content decreases over time.

DOI: 10.1021/acsami.9b04625
ACS Appl. Mater. Interfaces 2019, 11, 19819−19829

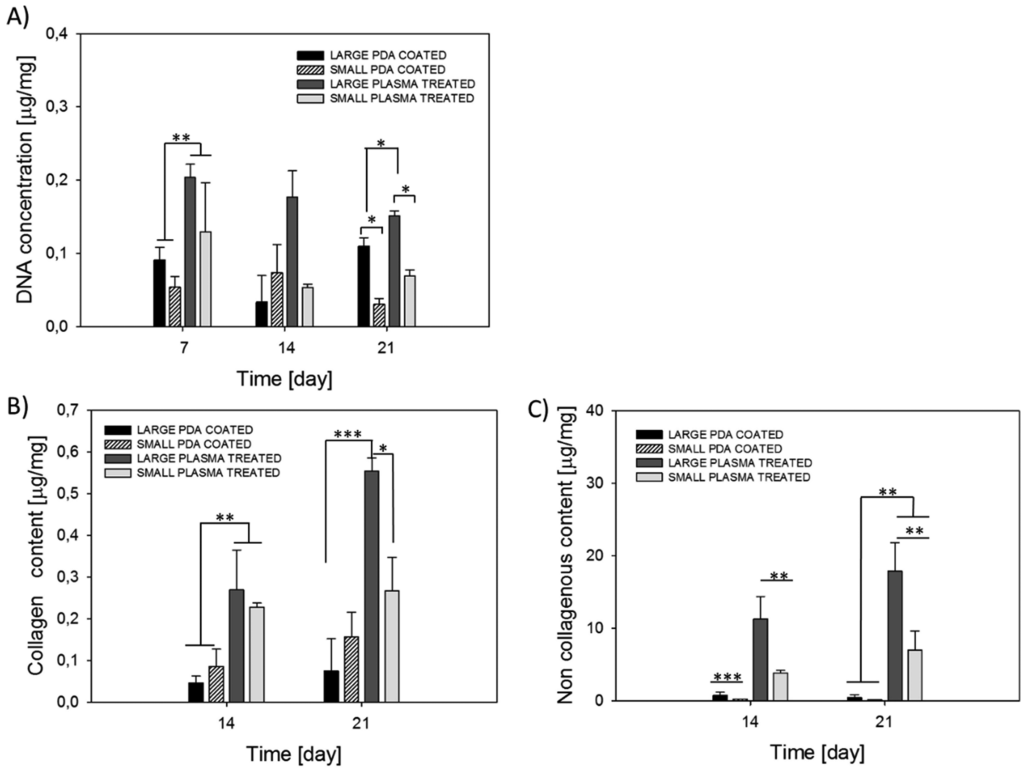

Figure 6. (A) DNA quantification of WJMSCs in PU scaffolds, either coated with PDA or treated with plasma (B) collagen secreted quantification in PU scaffold and (C) noncollagenous content secretion, values expressed as mean ± SD $n = 3$ $^{*}p < 0.05$, $^{**}p < 0.01$, $^{***}p < 0.001$.

Collagen and noncollagenous content are always significantly higher on plasma-treated samples compared to PDA-coated samples for a given interconnection size. For WJMSCs, ECM production is significantly higher on plasma-treated samples compared to PDA-coated ones. In the case of PDA-coated samples, almost no ECM production was observed. As far as DNA content is concerned, it is significantly higher over time on plasma-treated samples compared to PDA-coated ones, even if it is decreasing a bit over time. One does observe opposite behavior between fibroblasts and WJMSCs with respect to the surface treatment.

Hence, as demonstrated in Figures 3 and 4, surface functionalization improves the wettability of the PU scaffolds. As a result, cell suspension could clearly penetrate within the pores. Therefore, surface treatments allowed cells to colonize the scaffold in a preliminary way. Further interaction between the cells and the surface dictated the long-term response of the cells toward the PU surface. This was demonstrated to be rather cell specific.

In their respective favorable conditions, matrix synthesis by NIH 3T3 and WJMSCs is significantly higher for LARGE interconnections compared to SMALL ones, indicating the strong influence of the interconnection size on cell behavior.

We also performed confocal imaging of the scaffolds after 21 days of cell culture, where cells were stained with DAPI (blue) and phalloidin (red) to visualize the nuclei and the F-actin filaments, respectively. Typical images are shown in Figure 7 for NIH 3T3 cells and in Figure 8 for WJMSCs.

For both cells seeded on the favorable coated PU, scaffolds with LARGE interconnections are always more colonized than scaffold with SMALL ones. As far as NIH 3T3 cells are concerned, one observes that for LARGE interconnections, whole pores are colonized in the case of PDA treatment,

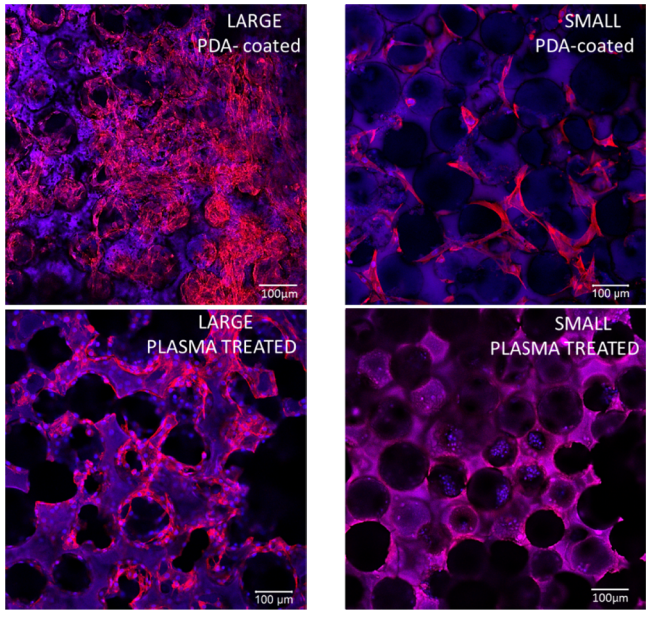

Figure 7. Confocal images of scaffolds seeded with NIH 3T3 Fibroblasts for 21 days of culture; cells were stained with DAPI (blue) for nucleus and phalloidin (red) for F-actin filament, images were taken in the center of the scaffold approximately.

whereas cells essentially colonize the surface of the pores for plasma-treated PU (Figure 7). After 24 h of culture, more fibroblasts were observed in structures with SMALL interconnections compared to day 21; for LARGE interconnections, no significant differences were seen between day 1 and day 21 (Figure S3). In the case of WJMSCs, cells fully colonize the plasma-treated PU with LARGE interconnections,

DOI: 10.1021/acsami.9b04625
ACS Appl. Mater. Interfaces 2019, 11, 19819−19829

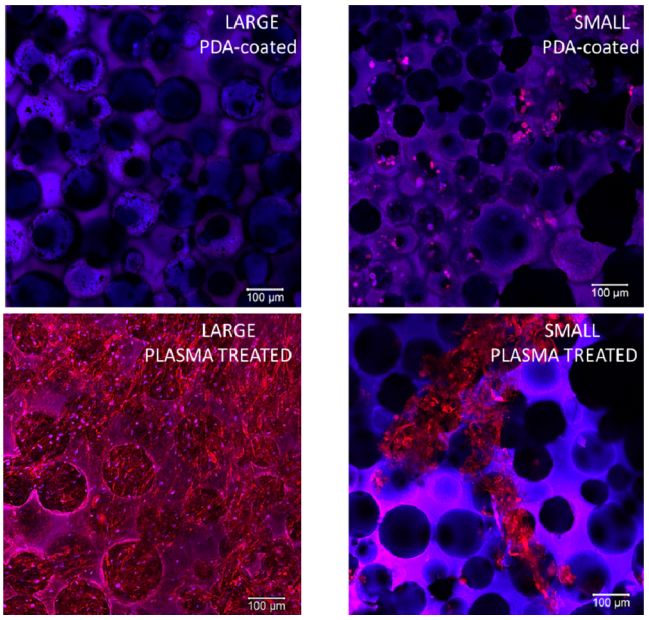

Figure 8. Confocal images of scaffolds seeded with WJMSCs for 21 days of culture; cells were stained with DAPI (blue) for nucleus and phalloidin (red) for F-actin filaments; images were taken in the center of the scaffold approximately.

whereas for SMALL interconnections, the material appears sparsely colonized. No colonization is observed when the PU was functionalized with PDA. These results are in agreement with those found by the DNA and ECM content analysis.

In order to obtain a better understanding of the colonization process, we also performed cell adhesion experiments on flat raw or functionalized PU surfaces (Figure S1 of the Supporting Information). Different behaviors occur with regard to the cell type. On plasma-treated PU, WJMSCs spread on the substrate after 1 day, but cells become round shaped after 2 days of culture (Figure S2 in the Supporting Information). On the other hand, fibroblasts poorly adhere on this substrate and present a tendency to form cell aggregates on the surface. One can, thus, conclude that WJMSCs and NIH 3T3 cells interact differently on the two substrates, but in any case, their adhesion appeared rather weak.

From our observations, one can conclude that despite weak adhesion, cells can colonize porous materials, synthesize ECM, and even totally fill the material. We find that interconnection size between different pores is of great importance, LARGE interconnections (larger than 50 μm) being needed for cell colonization. Moreover, we find that surface treatment plays an important role for cell colonization but must be adapted to the cell type.

4. DISCUSSION

Let us now discuss our results in the light of the literature. It has already been reported that when the cells have poor interactions with a biomaterial, they do secrete their own ECM on the surface of the material to create a more favorable environment. For instance, Ferreira et al.[43] produced a combination of sulfated modified-hyaluronic acid and polyethyleneglycol diacrylate hydrogel that did not contain any adhesion motifs, and they showed that human bone marrow mesenchymal stem cells secreted their own local pericellular ECM to which cells subsequently attached. One can assume that cells are able to create a local environment when they do not adhere directly on the material. Cells could, then, either recruit proteins from the serum or synthesize their own ECM to adhere on the material surface. This was shown on trimethylpropane trimethacrylate, where poorly adherent dental pulp stem cells showed an upregulation of collagen II, collagen IV, and vitronectin genes in serum-free conditions, which was attributed to a mechanism allowing the cells to remain attached on the material by their own secreted proteins.[44] For fibroblasts, collagen secretion was 0.2 ± 0.003 μg/mg on PDA-coated samples versus 0.1 ± 0.003 μg/mg on plasma-treated ones at day 14 in the case of LARGE interconnections (Figure 5B), and non-collagenous content was 5.6 ± 0.3 μg/mg on PDA-coated samples and 1.2 ± 0.08 μg/mg on plasma-treated samples at day 14 (Figure 5C). For all samples coated with PDA, both collagenous and non-collagenous secretion increased from day 14 to day 21, indicating the production of ECM by fibroblasts, whereas on plasma-treated PU, these contents remained constant.

For WJMSCs, there was only small collagen secretion with no noncollagenous secretions on PDA-treated PU, whereas significant secretions were observed on plasma-treated PU. In the latter case, an important increase in the secreted amounts of collagen (0.26 ± 0.09 to 0.56 ± 0.03 μg/mg) and noncollagen content (11.2 ± 3.12 to 18 ± 3.9 μg/mg) are observed between day 14 and day 21 for structures with LARGE interconnections (Figure 6B,C). This indicates strong ECM production, consistent with the entire pore colonization of NIH 3T3 cells on PDA-coated PU with LARGE interconnections and WJMSCs on plasma-treated PU with LARGE interconnections.

One can, thus, assume that in both cases, the interactions of the cells with the surface favors ECM production onto which cells can further attach, this process going on until the whole pores are filled. These findings demonstrate that the surface treatment can influence cell behavior and that this influence is highly dependent on cell type.

Our results also show that the size of the interconnections of the scaffolds has a significant influence on cell survival and on matrix production regardless of the surface modification. For both cell types, the DNA concentration is significantly higher in scaffolds with LARGE compared to SMALL interconnections (Figures 5A and 6A).

For instance, in PDA-coated PU structures, DNA concentration of fibroblasts at day 21 was 0.17 ± 0.002 μg/mg for LARGE interconnections, whereas it was only 0.07 ± 0.009 μg/mg for SMALL interconnections. Likewise, for WJMSCs, on plasma-treated PU with LARGE interconnections at day 21, DNA concentration was 0.15 ± 0.006 μg/mg, whereas it was 0.07 ± 0.008 μg/mg for SMALL interconnections.

Cellular organization was also checked by confocal images. In Figure 7, observations by confocal microscopy show that fibroblasts do not colonize the samples with SMALL interconnections either plasma-treated or PDA-coated. In the case of SMALL PDA-coated samples, only few cells after 21 days of culture are spread on the scaffold, whereas for SMALL plasma-treated samples, cells do not spread at all and have a rounded shape consistent with necrotic behavior. As previously explained, in samples with LARGE interconnections, fibroblasts react differently to surface treatments. In LARGE PDA-coated samples, cells fully colonized the pores after 21 days of culture with extensive spreading of their cytoplasm with elongated F-actin filaments. One can even observe that cells

DOI: 10.1021/acsami.9b04625
ACS Appl. Mater. Interfaces 2019, 11, 19819−19829

have been able to spread throughout the structure and create cell−cell contacts between adjacent pores. In LARGE plasma-treated samples, cells colonized the pores and remained generally on the outer part of the pores, thus favoring cell−substrate contacts instead of cell−cell contacts.

The effects of surface treatment and interconnection size are even more pronounced for WJMSCs (Figure 8). In PDA-coated samples with SMALL or LARGE interconnections, almost no cells were observed after 21 days of culture; they did not colonize the scaffold. On plasma-treated samples, the effect of interconnection size was more obvious because for LARGE interconnections, cells colonize the pores completely and spread throughout the entire structure also creating cell−cell contacts. In contrast, with SMALL interconnections, we can only observe few cells that spread across the scaffold, but most of the scaffold remains acellular. These data corroborated our quantitative findings which showed that LARGE PDA-coated scaffolds appear as the best substrate for 3T3 cells and LARGE plasma-treated scaffolds appear as the best substrate for WJMSCs.

The effect of interconnection size on cell behavior may be multifactorial and complex. LARGE interconnections may facilitate cell diffusion through the matrix. A typical cell size being of the order of a few to 10 μm, an interconnection size of 27 μm should allow for cell diffusion, but, when cells produce their matrix, it may become more difficult for cells to cross the interconnection. Moreover, larger interconnections should favor cell−cell communication between cells of adjacent pores. As discussed previously, the ECM produced by cells seems to play an important role in cell attachment and further cell behavior. But the significant difference in cell behavior with regard to the interconnection sizes can also be correlated to the transport properties as summarized in Table 1, where one observes that the hydraulic permeability is changing by 1 order of magnitude between scaffolds with 27 and 52 μm interconnections. As discussed previously, the interconnection diameter is the key parameter with regard to the hydraulic permeability that may affect the transport properties through the center of the scaffold. This may affect oxygen and nutrient supply in the center of the sample. This was reported by Kemppainen and Hollister[38] who generated PCL scaffolds in which permeability was controlled. Scaffold with the lowest permeability value showed higher cartilage matrix formation when seeded with chondrocytes compared with scaffolds having higher permeability values. These results were attributed to the lower oxygen tension that may promote cartilaginous matrix formation. Fan et al.[45] seeded MC-3T3-E1 cells on tricalcium phosphate scaffolds with varying permeability. Under static culture conditions, they found that cell survival was enhanced in the scaffold with the highest permeability even if the effect was more pronounced under flow perfusion. Again, the authors reported that permeability affects the transport properties with regard to both the nutrients and oxygen supply to the center of the scaffold, and the waste removal, which may drastically lower the local pH value. Moreover, cellular growth on porous scaffold is thought to be faster for cells on the outer surface than for cells in the deeper layers because on the outside, cells have a better access to nutrients. For instance, Galban and Locke[46] gave a mathematical approach to describe cell growth in a porous polymer. They proposed that cells located on the outer surface will grow more rapidly than the cells located deeper in the scaffold due to a higher nutrient supply. They argued that cells on the outer surface will merge and finally cover the whole surface. At this point, nutrient supply inside the construct will be limited by diffusion through the cell layer before reaching the cells inside the scaffold.

Let us finish by discussing the effect of PDA on cell adhesion. We observe that PDA-treatment of the PU scaffold is favorable for NIH-3T3 proliferation inside the material, whereas it does not allow WJMSCs to proliferate. PDA structure on surfaces is still not well understood. Some authors are considering it as an assembly of supramolecular aggregates rather than a polymer.[47] This material derived from mussel foot protein can virtually bind to any kind of surface through its catecholamine groups such as dopamine. Over the last 10 years, functionalization with PDA layer has been used to promote cell adhesion on different substrates such as polydimethylsiloxane,[48] PCL,[49] PLGA[49] or PU.[50] This PDA layer has been shown to promote serum protein adsorption and thus provide an adhesion motif for cells to attach and grow.[48] However, the adsorption of serum proteins alone could not explain cell proliferation and growth on such a substrate as many studies have demonstrated that the adhesion on PDA depends on cell type. It has been found that dopamine induces human adipose derived stem cells proliferation on PLGA-coated substrate, whereas it did not have any effect on polystyrene. It was also shown that PDA-coated PLGA did not promote proliferation of other cell types, such as human umbilical vein endothelial cells or induced pluripotent stem cells.[51] These results are consistent with our study and highlight the complexity of cell adhesion processes on solid surfaces. WJMSCs were already seeded onto a PDA-modified calcium silicate/PCL composite scaffold.[52] No significant proliferation was found with respect to the control which was WJMSCs seeded on a 2D plate for 7 days. This indicates that PDA alone did not promote stem cells proliferation in other porous substrates. However, in another study, dopamine-coated calcium silicate surface was shown to increase WJMSCs adhesion for 7 days and β-1 integrin expression was also higher on the dopamine-coated surface.[53] These results clearly demonstrate that the mechanism through which a defined cell type can or cannot adhere and proliferate on PDA layer is yet to be understood.

5. CONCLUSIONS

The physicochemical properties of porous scaffolds significantly affect their ability to integrate with the host tissue via ingrowth of the connective tissue cells. Here, we have introduced a scaffold production protocol which can control the interconnections of the pores while keeping the pore size constant in PU scaffolds. The interconnections significantly affect cell distribution and ECM secretion, when coupled with either plasma or PDA surface treatments in a cell type dependent manner. The extent and response to the surface treatments were different for WJMSCs where plasma treatment enhanced cell colonization, and fibroblasts where it was the PDA treatment that favored cell colonization. The effect of interconnection was equally important for both stem cells and fibroblasts where colonization and cell growth were promoted by LARGER interconnections most likely due to the significantly improved permeability and ease of cellular connections within 3D structures. Precise control of pore interconnectivity at microscale and surface properties in nanoscale could provide optimized 3D scaffolds for both cell migration and differentiation. Dynamic culture conditions are

DOI: 10.1021/acsami.9b04625
ACS Appl. Mater. Interfaces 2019, 11, 19819−19829

considered for further work to better harness the improved transport properties of scaffolds with LARGE interconnections.

■ ASSOCIATED CONTENT

Supporting Information

The Supporting Information is available free of charge on the ACS Publications website at DOI: 10.1021/acsami.9b04625.

Images taken with an optical microscope of WJMSCs and 3T3 fibroblasts on PU flat surfaces after 24 h; images taken with an optical microscope of WJMSCs and 3T3 fibroblasts on PU flat surfaces after 48 h; confocal images of NTH 3T3 fibroblast in PU scaffolds after 24 h of culture; and typical stress−strain curve of the scaffold with both SMALL and LARGE interconnections (PDF)

■ AUTHOR INFORMATION

Corresponding Authors

*E-mail: glutzweiler@hotmail.fr (G.L.).
*E-mail: schaaf@unistra.fr (P.S.).
*E-mail: e.vrana@protipmedical.com (N.E.V.).

ORCID

H. Kerdjoudj: 0000-0002-8072-9728
F. Boulmedais: 0000-0002-4934-9276
P. Schaaf: 0000-0001-7423-5492
N. E. Vrana: 0000-0002-5398-6710

Author Contributions

The manuscript was written through contributions of all authors. All authors have given approval to the final version of the manuscript.

Funding

The authors received financial supports from the Horizon 2020 PANBioRA grant (grant agreement no. 760921), and from MICA DiarARTother. This work has been published within the IdEx Unistra framework (Attractivity Chair W. Drenckhan) and has benefited from funding from the state, managed by the French National Research Agency as part of the "Investments for the future" program. The authors also received funding from the doctoral school of physics and physical chemistry of the University of Strasbourg as well as from the French National Research Agency.

Notes

The authors declare no competing financial interest.

■ ACKNOWLEDGMENTS

The authors thank Horizon 2020 PANBioRA (grant agreement no. 760921), Institut Carnot MICA through the project DiaART as well as the grant of doctoral school of physics and physical chemistry of Strasbourg (G.L.). Thanks to Robin Bollache and Leandro Jacomine for technical help. The authors thank FoamPartner company for the kind supply of products as well as for the regular discussions. The authors would like to thank the microscopy platform and especially Marc Schmutz and Alain Carvalho for fruitful discussions.

■ ABBREVIATIONS

PU, polyurethane
PDA, polydopamine
WJMSCS, Wharton's jelly mesenchymal stem cells
ECM, extracellular matrix
GAGs, glycoaminoglycans

■ REFERENCES

(1) Karp, J. M.; Dalton, P. D.; Shoichet, M. S. Scaffolds for Tissue Engineering. *MRS Bull.* **2003**, *28*, 301−306.
(2) Karageorgiou, V.; Kaplan, D. Porosity of 3D Biomaterial Scaffolds and Osteogenesis. *Biomaterials* **2005**, *26*, 5474−5491.
(3) Hutmacher, D. W. Scaffolds in Tissue Engineering Bone and Cartilage. *Biomaterials* **2000**, *21*, 2529−2543.
(4) Vrana, N. E.; Liu, Y.; McGuinness, G. B.; Cahill, P. A. Characterization of Poly(Vinyl Alcohol)/Chitosan Hydrogels as Vascular Tissue Engineering Scaffolds. *Macromol. Symp.* **2008**, *269*, 106−110.
(5) Vrana, N. E.; Dupret, A.; Coraux, C.; Vautier, D.; Debry, C.; Lavalle, P. Hybrid Titanium/Biodegradable Polymer Implants with an Hierarchical Pore Structure as a Means to Control Selective Cell Movement. *PLoS One* **2011**, *6*, No. e20480.
(6) Jafari, M.; Paknejad, Z.; Rad, M. R.; Motamedian, S. R.; Eghbal, M. J.; Nadjmi, N.; Khojasteh, A. Polymeric Scaffolds in Tissue Engineering: A Literature Review. *J. Biomed. Mater. Res., Part B* **2017**, *105*, 431−459.
(7) Laschke, M. W.; Harder, Y.; Amon, M.; Martin, I.; Farhadi, J.; Ring, A.; Torio-Padron, N.; Schramm, R.; Rücker, M.; Junker, D.; Häufel, J. M.; Carvalho, C.; Heberer, M.; Germann, G.; Vollmar, B.; Menger, M. D. Angiogenesis in Tissue Engineering: Breathing Life into Constructed Tissue Substitutes. *Tissue Eng.* **2006**, *12*, 2093−2104.
(8) Bil, M.; Ryszkowska, J.; Kurzydłowski, K. J. Effect of Polyurethane Composition and the Fabrication Process on Scaffold Properties. *J. Mater. Sci.* **2009**, *44*, 1469−1476.
(9) Hafeman, A. E.; Li, B.; Yoshii, T.; Zienkiewicz, K.; Davidson, J. M.; Guelcher, S. A. Injectable Biodegradable Polyurethane Scaffolds with Release of Platelet-Derived Growth Factor for Tissue Repair and Regeneration. *Pharm. Res.* **2008**, *25*, 2387−2399.
(10) Lv, Q.; Feng, Q. Preparation of 3-D Regenerated Fibroin Scaffolds with Freeze Drying Method and Freeze Drying/Foaming Technique. *J. Mater. Sci. Mater. Med.* **2006**, *17*, 1349−1356.
(11) Hung, K.-C.; Tseng, C.-S.; Hsu, S.-h. Synthesis and 3D Printing of Biodegradable Polyurethane Elastomer by a Water-Based Process for Cartilage Tissue Engineering Applications. *Adv. Healthc. Mater.* **2014**, *3*, 1578−1587.
(12) Oh, S. H.; Kim, T. H.; Im, G. I.; Lee, J. H. Investigation of Pore Size Effect on Chondrogenic Differentiation of Adipose Stem Cells Using a Pore Size Gradient Scaffold. *Biomacromolecules* **2010**, *11*, 1948−1955.
(13) O'Brien, F. J.; Harley, B. a.; Yannas, I. V.; Gibson, L. J. The Efect of Pore Size on Cell Adhesion in Collagen GAG Scaffolds. *Biomaterials* **2005**, *26*, 433−441.
(14) Sobral, J. M.; Caridade, S. G.; Sousa, R. A.; Mano, J. F.; Reis, R. L. Three-Dimensional Plotted Scaffolds with Controlled Pore Size Gradients: Effect of Scaffold Geometry on Mechanical Performance and Cell Seeding Efficiency. *Acta Biomater.* **2011**, *7*, 1009−1018.
(15) Costantini, M.; Colosi, C.; Jaroszewicz, J.; Tosato, A.; Święszkowski, W.; Dentini, M.; Garstecki, P.; Barbetta, A. Microfluidic Foaming: A Powerful Tool for Tailoring the Morphological and Permeability Properties of Sponge-like Biopolymeric Scaffolds. *ACS Appl. Mater. Interfaces* **2015**, *7*, 23660−23671.
(16) Pamula, E.; Bacakova, L.; Filova, E.; Buczynska, J.; Dobrzynski, P.; Noskova, L.; Grausova, L. The Influence of Pore Size on Colonization of Poly(l-Lactide-Glycolide) Scaffolds with Human Osteoblast-like MG 63 Cells in Vitro. *J. Mater. Sci. Mater. Med.* **2008**, *19*, 425−435.
(17) Stenhamre, H.; Nannmark, U.; Lindahl, A.; Gatenholm, P.; Brittberg, M. Influence of Pore Size on the Redifferentiation Potential of Human Articular Chondrocytes in Poly(Urethane Urea) Scaffolds. *J. Tissue Eng. Regener. Med.* **2010**, *5*, 578−588.
(18) Matsiko, A.; Gleeson, J. P.; O'Brien, F. J. Scaffold Mean Pore Size Influences Mesenchymal Stem Cell Chondrogenic Differentiation and Matrix Deposition. *Tissue Eng., Part A* **2015**, *21*, 486−497.
(19) Reinwald, Y.; Johal, R. K.; Ghaemmaghami, A. M.; Rose, F. R. A. J.; Howdle, S. M.; Shakesheff, K. M. Interconnectivity and

DOI: 10.1021/acsami.9b04625
ACS Appl. Mater. Interfaces 2019, 11, 19819−19829

Permeability of Supercritical Fluid-Foamed Scaffolds and the Effect of Their Structural Properties on Cell Distribution. *Polymer* **2014**, *55*, 435−444.
(20) Mastrogiacomo, M.; Scaglione, S.; Martinetti, R.; Dolcini, L.; Beltrame, F.; Cancedda, R.; Quarto, R. Role of Scaffold Internal Structure on in Vivo Bone Formation in Macroporous Calcium Phosphate Bioceramics. *Biomaterials* **2006**, *27*, 3230−3237.
(21) Madden, L. R.; Mortisen, D. J.; Sussman, E. M.; Dupras, S. K.; Fugate, J. A.; Cuy, J. L.; Hauch, K. D.; Laflamme, M. A.; Murry, C. E.; Ratner, B. D. Proangiogenic Scaffolds as Functional Templates for Cardiac Tissue Engineering. *Proc. Natl. Acad. Sci. U.S.A.* **2010**, *107*, 15211−15216.
(22) Ma, P. X.; Choi, J.-W. Biodegradable Polymer Scaffolds with Well-Defined Interconnected Spherical Pore Network. *Tissue Eng.* **2001**, *7*, 23−33.
(23) Oloffs, A.; Grosse-Siestrup, C.; Bisson, S.; Rinck, M.; Rudolph, R.; Gross, U. Biocompatibility of silver-coated polyurethane catheters and silvercoated Dacron material. *Biomaterials* **1994**, *15*, 753−758.
(24) Laschke, M. W.; Strohe, A.; Scheuer, C.; Eglin, D.; Verrier, S.; Alini, M.; Pohlemann, T.; Menger, M. D. In vivo biocompatibility and vascularization of biodegradable porous polyurethane scaffolds for tissue engineering. *Acta Biomater.* **2009**, *5*, 1991−2001.
(25) Li, Z.; Yao, S.-J.; Alini, M.; Stoddart, M. J. Chondrogenesis of Human Bone Marrow Mesenchymal Stem Cells in Fibrin−Polyurethane Composites Is Modulated by Frequency and Amplitude of Dynamic Compression and Shear Stress. *Tissue Eng., Part A* **2010**, *16*, 575−584.
(26) Li, Y.-H.; Huang, Y.-D. The Study of Collagen Immobilization on Polyurethane by Oxygen Plasma Treatment to Enhance Cell Adhesion and Growth. *Surf. Coating. Technol.* **2007**, *201*, 5124−5127.
(27) Lin, H.-B.; Sun, W.; Mosher, D. F.; García-Echeverría, C.; Schaufelberger, K.; Lelkes, P. I.; Cooper, S. L. Synthesis, Surface, and Cell-Adhesion Properties of Polyurethanes Containing Covalently Grafted RGD-Peptides. *J. Biomed. Mater. Res.* **1994**, *28*, 329−342.
(28) Lee, H. Mussel-Inspired Surface Chemistry for Multifunctionnal Coatings. *Science* **2007**, *318*, 426−430.
(29) Ku, S. H.; Park, C. B. Human Endothelial Cell Growth on Mussel-Inspired Nanofiber Scaffold for Vascular Tissue Engineering. *Biomaterials* **2010**, *31*, 9431−9437.
(30) Tsai, W.-B.; Chen, W.-T.; Chien, H.-W.; Kuo, W.-H.; Wang, M.-J. Poly(Dopamine) Coating of Scaffolds for Articular Cartilage Tissue Engineering. *Acta Biomater.* **2011**, *7*, 4187−4194.
(31) Grenier, S.; Sandig, M.; Mequanint, K. Polyurethane Biomaterials for Fabricating 3D Porous Scaffolds and Supporting Vascular Cells. *J. Biomed. Mater. Res. A* **2007**, *82*, 802−809.
(32) Loh, Q. L.; Choong, C. Three-Dimensional Scaffolds for Tissue Engineering Applications: Role of Porosity and Pore Size. *Tissue Eng., Part B* **2013**, *19*, 485−502.
(33) Marshall, A. J.; Ratner, B. D. Quantitative Characterization of Sphere-Templated Porous Biomaterials. *AIChE J.* **2005**, *51*, 1221−1232.
(34) Pennella, F.; Cerino, G.; Massai, D.; Gallo, D.; Falvo D'Urso Labate, G.; Schiavi, A.; Deriu, M. A.; Audenino, A.; Morbiducci, U. A Survey of Methods for the Evaluation of Tissue Engineering Scaffold Permeability. *Ann. Biomed. Eng.* **2013**, *41*, 2027−2041.
(35) Smith, J. R.; Pfeifer, K.; Petry, F.; Powell, N.; Delzeit, J.; Weiss, M. L. Standardizing Umbilical Cord Mesenchymal Stromal Cells for Translation to Clinical Use: Selection of GMP-Compliant Medium and a Simplified Isolation Method. *Stem Cell. Int.* **2016**, *2016*, 1−14.
(36) Schneider, C. A.; Rasband, W. S.; Eliceiri, K. W. NIH Image to ImageJ: 25 Years of Image Analysis. *Nat. Methods* **2012**, *9*, 671−675.
(37) Chor, M. V.; Li, W. A Permeability Measurement System for Tissue Engineering Scaffolds. *Meas. Sci. Technol.* **2007**, *18*, 208−216.
(38) Kemppainen, J. M.; Hollister, S. J. Differential Effects of Designed Scaffold Permeability on Chondrogenesis by Chondrocytes and Bone Marrow Stromal Cells. *Biomaterials* **2010**, *31*, 279−287.
(39) Myung, S.-W.; Yeom, Y.-H.; Jang, Y.-M.; Choi, H.-S.; Cho, D. Preparation of a Reticulated Polyurethane Foam Grafted with Poly(Acrylic Acid) through Atmospheric Pressure Plasma Treatment and Its Lysozyme Immobilization. *J. Mater. Sci. Mater. Med.* **2005**, *16*, 745−751.
(40) Sanchis, M. R.; Calvo, O.; Fenollar, O.; Garcia, D.; Balart, R. Characterization of the Surface Changes and the Aging Effects of Low-Pressure Nitrogen Plasma Treatment in a Polyurethane Film. *Polym. Test.* **2008**, *27*, 75−83.
(41) Sanchis, M. R.; Calvo, O.; Fenollar, O.; Garcia, D.; Balart, R. Surface Modification of a Polyurethane Film by Low Pressure Glow Discharge Oxygen Plasma Treatment. *J. Appl. Polym. Sci.* **2007**, *105*, 1077−1085.
(42) Della Vecchia, N. F.; Luchini, A.; Napolitano, A.; D'Errico, G.; Vitiello, G.; Szekely, N.; d'Ischia, M.; Paduano, L. Tris Buffer Modulates Polydopamine Growth, Aggregation, and Paramagnetic Properties. *Langmuir* **2014**, *30*, 9811−9818.
(43) Ferreira, S. A.; Motwani, M. S.; Faull, P. A.; Seymour, A. J.; Yu, T. T. L.; Enayati, M.; Taheem, D. K.; Salzlechner, C.; Haghighi, T.; Kania, E. M.; OOmen, O. P. Bi-Directional Cell-Pericellular Matrix Interactions Direct Stem Cell Fate. *Nat. Commun.* **2018**, *9*, 4049.
(44) Vining, K. H.; Scherba, J. C.; Bever, A. M.; Alexander, M. R.; Celiz, A. D.; Mooney, D. J. Synthetic Light-Curable Polymeric Materials Provide a Supportive Niche for Dental Pulp Stem Cells. *Adv. Mater.* **2018**, *30*, 1704486.
(45) Fan, J.; Jia, X.; Huang, Y.; Fu, B. M.; Fan, Y. Greater Scaffold Permeability Promotes Growth of Osteoblastic Cells in a Perfused Bioreactor. *J. Tissue Eng. Regener. Med.* **2013**, *9*, E210−E218.
(46) Galban, C. J.; Locke, B. R. Analysis of Cell Growth in a Polymer Scaffold Using a Moving Boundary Approach. *Biotechnol. Bioeng.* **1997**, *56*, 422−432.
(47) Bernsmann, F.; Ball, V.; Addiego, F.; Ponche, A.; Michel, M.; Gracio, J. J. d. A.; Toniazzo, V.; Ruch, D. Dopamine−Melanin Film Deposition Depends on the Used Oxidant and Buffer Solution. *Langmuir* **2011**, *27*, 2819−2825.
(48) Ku, S. H.; Lee, J. S.; Park, C. B. Spatial Control of Cell Adhesion and Patterning through Mussel-Inspired Surface Modification by Polydopamine. *Langmuir* **2010**, *26*, 15104−15108.
(49) Jo, S.; Kang, S. M.; Park, S. A.; Kim, W. D.; Kwak, J.; Lee, H. Enhanced Adhesion of Preosteoblasts inside 3DPCL Scaffolds by Polydopamine Coating and Mineralization. *Macromol. Biosci.* **2013**, *13*, 1389−1395.
(50) Davoudi, P.; Assadpour, S.; Derakhshan, M. A.; Ai, J.; Solouk, A.; Ghanbari, H. Biomimetic Modification of Polyurethane-Based Nanofibrous Vascular Grafts: A Promising Approach towards Stable Endothelial Lining. *Mater. Sci. Eng., C* **2017**, *80*, 213−221.
(51) Yang, K.; Lee, J. S.; Kim, J.; Lee, Y. B.; Shin, H.; Um, S. H.; Kim, J. B.; Park, K. I.; Lee, H.; Cho, S.-W. Polydopamine-Mediated Surface Modification of Scaffold Materials for Human Neural Stem Cell Engineering. *Biomaterials* **2012**, *33*, 6952−6964.
(52) Chen, Y.-W.; Shen, Y.-F.; Ho, C.-C.; Yu, J.; Wu, Y.-H. A.; Wang, K.; Shih, C.-T.; Shie, M.-Y. Osteogenic and Angiogenic Potentials of the Cell-Laden Hydrogel/Mussel-Inspired Calcium Silicate Complex Hierarchical Porous Scaffold Fabricated by 3D Bioprinting. *Mater. Sci. Eng., C* **2018**, *91*, 679−687.
(53) Kao, C.-T.; Chen, Y.-J.; Ng, H.-Y.; Lee, A.; Huang, T.-H.; Lin, T.-F.; Hsu, T.-T. Surface Modification of Calcium Silicate via Mussel-Inspired Polydopamine and Effective Adsorption of Extracellular Matrix to Promote Osteogenesis Differentiation for Bone Tissue Engineering. *Materials* **2018**, *11*, 1664.

DOI: 10.1021/acsami.9b04625
ACS Appl. Mater. Interfaces 2019, 11, 19819−19829